Journal of Nuclear Materials 396 (2010) 107–111

Contents lists available at ScienceDirect

Journal of Nuclear Materials

journal homepage: www.elsevier.com/locate/jnucmat

^{17}O NMR study in $(Pu_{0.91}Am_{0.09})O_2$

Yo Tokunaga [a,*], Masahiko Osaka [b], Shinsaku Kambe [a], Shuhei Miwa [b], Hironori Sakai [a], Hiroyuki Chudo [a], Yoshiya Homma [c], Yoshinobu Shiokawa [c]

[a] Advanced Science Research Center, Japan Atomic Energy Agency, Tokai, Naka, Ibaraki 319-1195, Japan
[b] Oarai Research and Development Center, Japan Atomic Energy Agency, Oarai, Higashi-Ibaraki, Ibaraki 311-1393, Japan
[c] Institute for Materials Research, Tohoku University, Oarai, Higashi-Ibaraki, Ibaraki 311-1313, Japan

ARTICLE INFO

Article history:
Received 19 May 2009
Accepted 28 October 2009

Keywords:
Plutonium dioxide
Americium dioxide
^{17}O NMR
Magnetic moment

ABSTRACT

In order to investigate the magnetic properties of Am^{4+} ions in the cubic fluorite structure, we have performed ^{17}O NMR measurements on $(Pu_{0.91}Am_{0.09})O_2$. We have observed a temperature-dependent ^{17}O NMR line broadening induced by classical dipolar hyperfine fields from the Am 5*f* moments. From NMR line simulations, the effective moment of the Am moments has been estimated to be $\mu_{eff} = 1.38\mu_B$/Am. This value is comparable with $\mu_{eff} = 1.32$ or $1.53\mu_B$/Am reported for AmO_2. We have also carried out nuclear relaxation measurements for ^{17}O nuclei. The magnetization recovery has been found to exhibit a nonexponential time dependence with an exponent $\beta \sim 0.5$. This result is well understood in terms of the nuclear relaxation mechanism induced by the Am 5*f* moment fluctuations via dipolar hyperfine fields.

1. Introduction

Actinide dioxides (AnO_2: An = U, Np, Pu, and Am etc.) represent possibly the most intensely studied series of any actinide compounds. From chemical and industrial perspectives, this interest has stemmed from their use as nuclear fuels. Recently, however, AnO_2 has attracted a great deal of attention in the field of *f*-electron physics. Their surprisingly varied physical properties stimulate continuing interest for both theory and experiment. All the actinide ions in AnO_2 have the same tetravalent state, so that the number of localized *f*-electrons per actinide ion varies systematically, with two for U^{4+}, three for Np^{4+} and four for Pu^{4+} in the same cubic fluorite structure. In addition, in *f*-electron systems, real spin and orbital are not independent degrees of freedom, since they are tightly coupled with each other. Then, in order to describe such a complicated spin–orbital coupled system, it is rather appropriate to represent the *f*-electron state in terms of "multipole" degrees of freedom. Available multipoles on each material are dependent on the number of *f*-electrons as well as the symmetry of the crystal. In the cubic symmetry of AnO_2, even the higher order multipoles (quadrupole and octupole) are not quenched, and are found to affect the physical properties at low temperatures.

In order to investigate the electronic state of AnO_2 from a microscopic viewpoint, we have performed a series of nuclear magnetic resonance (NMR) studies using ^{17}O nuclei [1–8]. The advantage of NMR experiments is that the static and dynamical electronic properties can be selectively probed for each site in a given compound. In the ordered state of UO_2, for example, the ^{17}O NMR has revealed the existence of a large internal field with a tiny electronic field gradient at oxygen sites [1,6,7]. These results have confirmed the transverse triple-*q* type ordering of magnetic dipoles in UO_2. In NpO_2, on the other hand, the ^{17}O NMR data has provided clear evidence for novel magnetic order associated with octupole degree of freedom [2,4,8]. In addition, spin–lattice relaxation rate $(1/T_1)$ measurements have revealed the occurrence of a cross relaxation process between the ^{237}Np 5*f* spins and the ^{17}O nuclei via a greatly enhanced indirect nuclear spin–spin coupling [9]. From the ^{17}O NMR studies, clear distinctions between the electronic states of UO_2, NpO_2, and PuO_2 have been obtained.

AmO_2 is known to exhibit an exotic phase transition at 8.5 K [10]. However, due to a limited number of experimental data for AmO_2, the mechanism of this phase transition remains a mystery more than 30 years [11,12]. In order to clarify the mechanism of the phase transition, it is important to promote a better understanding of the magnetic properties of Am^{4+} ions in the cubic fluorite structure. For this purpose, we extend our ^{17}O NMR studies to Am doped PuO_2. Note that the study of the Am doped PuO_2 is also important from the technological perspective. It is a candidate form of minor actinide including oxides of the target for both a fast reactor [13] and/or an accelerator driven sub-critical system [14]. The knowledge of the fundamental properties would support a basic interpretation of a complicated nuclear fuel system, e.g. the ef-

* Corresponding author. Address: Advanced Science Research Center, Japan Atomic Energy Agency, 2-4 Shirakata-Shirane, Tokai, Naka, Ibaraki 319-1195, Japan.
E-mail address: tokunaga.yo@jaea.go.jp (Y. Tokunaga).

0022-3115/$ - see front matter © 2009 Elsevier B.V. All rights reserved.
doi:10.1016/j.jnucmat.2009.10.062

fects of Am addition on the physical properties of the standard fuel, irradiation behavior, and so on.

2. Experimental

2.1. Sample preparation

A $(Pu_{0.91}Am_{0.09})^{17}O_2$ sample for the NMR measurements was prepared by oxidation of $(Pu_{0.91}Am_{0.09})N$ using isotopic-enriched gas $^{17}O_2$. About 9 mg of the starting material, $(Pu_{0.91}Am_{0.09})^{16}O_2$, was converted to $(Pu_{0.91}Am_{0.09})N$ by the carbothermic reduction process [15]. Americium in the $(Pu_{0.91}Am_{0.09})^{16}O_2$ powder was derived from ^{241}Pu. The $(Pu_{0.91}Am_{0.09})^{16}O_2$ was thoroughly mixed and milled with reagent grade graphite powder (Wako Pure Chemical Industries Ltd.) in an agate mortar with a pestle. The molar ratio of C to metal (Pu+Am) was three. The mixed powder was then pressed into a columnar pellet. Heat treatment of the compacted pellet was carried out in flowing N_2 gas for 5 h at 1673 K for carbothermic reduction and conversion of $(Pu_{0.91}Am_{0.09})^{16}O_2$ into $(Pu_{0.91}Am_{0.09})N$. Subsequent heat treatment in N_2/4% H_2 gas for 4 h at 1673 K was then done in order to remove the residual graphite. The $(Pu_{0.91}Am_{0.09})N$ so obtained, in which no ^{16}O was included, was then heat treated in 90% ^{17}O enriched O_2 gas for 1.5 h at 1273 K. The Am content in the sample was determined from a chemical analysis result of the powder, considering the possible loss of Am during the heat-treatment process evaluated from a preliminary study by the authors. Although no X-ray diffraction analysis of the prepared $(Pu_{0.91}Am_{0.09})^{17}O_2$ was carried out on account of the small amount of sample, it is believed that the prepared $(Pu_{0.91}Am_{0.09})^{17}O_2$ was well crystallized in view of the results of a similar test using CeO_2 as a surrogate of (Pu, Am)O_2 that was prepared from CeN using the same procedure; X-ray diffraction peaks of the CeO_2 sample indicated the fluorite-type structure without any peaks derived from impurities.

2.2. NMR measurements

The $(Pu_{0.91}Am_{0.09})O_2$ powder was wrapped with polyimide tape and encapsulated in a polyimide tube using epoxy resin. The encapsulated sample in the tube was doubly sealed in a Teflon capsule using epoxy resin, and then mounted into an rf coil and settled at the center of a superconducting magnet installed in a special area for handling radioisotopes. ^{17}O NMR measurements were carried out using a phase coherent, pulsed spectrometer. The ^{17}O nucleus has $I = 5/2$ with a gyromagnetic ratio $\gamma_N = 5.7719$ MHz/T, and thus possess a nuclear quadrupole moment. The NMR spectrum was obtained from fast Fourier transformation (FFT) of spin-echo profiles under an external magnetic field of $H_0 = 51.51$ kOe. The spin–lattice relaxation time T_1 was measured on the same powder sample using the saturation–recovery method.

3. Results and discussion

3.1. NMR spectrum

Fig. 1 shows a series of ^{17}O NMR spectra at temperatures of 10, 20, 35, 55, and 86 K, respectively. The NMR spectra broaden gradually with decreasing temperature, while they do not change their peak position at the frequency $f \simeq \gamma_N H_0$ for the whole temperature range. There are no satellite peaks associated with a quadrupole splitting, reflecting the cubic symmetry at the oxygen positions.

In Fig. 2, we plot the full widths at half maximum of the NMR spectra, Δf, against temperature. The temperature dependence of Δf is well reproduced by the sum of a Curie–Weiss (CW) term and a constant term, that is,

$$\Delta f(\mathrm{kHz}) = \frac{C}{T+\theta} + f_0, \tag{1}$$

as shown by the solid line in Fig. 2. The existence of the CW term reveals that the temperature-dependent part of the NMR line broadening is due to an interaction with localized magnetic moments. Similar temperature-dependent line broadening has been observed recently in Gd-doped CeO_2, where a fraction of the nonmagnetic Ce atoms is substituted with magnetic Gd atoms [16]. On the other hand, in fitting the data, a temperature-independent line width $f_0 = 14.4$ kHz was also obtained. This f_0 term tells us that there are other sources of line broadening existing even at high temperatures. It is supposed that a part of the f_0 term arises from lattice distortions or defects induced by radiation damage. The imperfections of the cubic lattice are known to cause tiny electronic field gradients at the O sites, which lead to NMR line broadening through quadrupolar interactions [1,4].

Note that PuO_2 is known to exhibit a temperature-independent magnetic susceptibility ($\chi(T)$), reflecting the non-magnetic Γ_1 crystal electric field (CEF) ground state of the Pu^{4+} ions [17–20]. On the other hand, $\chi(T)$ for AmO_2 shows CW behavior in the paramagnetic state. The CEF ground state of $Am^{4+}(5f^5)$ has been considered to be the magnetic Γ_7 doublet and likewise for the isoelectronic Pu^{3+} [10,21]. Recently, however, a possibility of the magnetic Γ_8 quartet ground state due to the competition between Coulomb interactions and spin–orbit coupling has been pointed out [22]. In either case, the CEF ground state is magnetic. Therefore, it would be natural to consider that the CW term in Eq. (1) originates from the magnetic (dipole) moment carried by Am 5*f* electrons. The magnetic moments can be coupled with ^{17}O nuclei through magnetic interactions and thus become a source of NMR line broadening as discussed below.

In AnO_2, the ^{17}O nuclei are regarded as belonging to ligand sites, which have no intrinsic magnetic moment. In such a case, the nuclear spin Hamiltonian of ^{17}O may be written using the dipolar hyperfine field $\boldsymbol{H}_{\mathrm{dip}}$ and the second rank Knight shift tensor $\tilde{K}$ as,

$$\mathscr{H}^{spin} = -\gamma_N \hbar \boldsymbol{I}\cdot\boldsymbol{H}_0 - \gamma_N \hbar \boldsymbol{I}\cdot\boldsymbol{H}_{\mathrm{dip}} - \gamma_N \hbar[\boldsymbol{I}\cdot\tilde{K}\cdot\boldsymbol{H}_0]. \tag{2}$$

The first term is due to the Zeeman interaction between the nuclear spin $\boldsymbol{I}$ and the applied field $\boldsymbol{H}_0$. The second term is the classical dipolar hyperfine interaction arising from the 5*f* spin moments of An ions. The third term is the so-called transferred hyperfine interaction arising from the on-site spin density at O sites as a consequence of the orbital hybridization effect between An 5*f* and O 2*p* electrons. For AnO_2, however, the transferred term is expected to be relatively small compared with the other two terms, since the AnO_2 are all insulators and thus the 5*f* electrons are well-localized. This has been confirmed with ^{17}O NMR in the ordered state of UO_2 [1]. If the transferred term is neglected in Eq. (2), the NMR frequency f_N is simply given by

$$f_N = \gamma_N(H_0 + H'_{\mathrm{dip}}), \tag{3}$$

since $\boldsymbol{H}_{\mathrm{dip}} \ll \boldsymbol{H}_0$. Here H'_{dip} is the projection of $\boldsymbol{H}_{\mathrm{dip}}$ along $\boldsymbol{H}_0$, i.e. $H'_{\mathrm{dip}} = H_{\mathrm{dip}}\cos\theta$, where θ is the angle between $\boldsymbol{H}_{\mathrm{dip}}$ and $\boldsymbol{H}_0$. Therefore, if there is no other source of NMR line broadening, a NMR line profile directly corresponds to a histogram of H'_{dip} at nuclear sites.

The dipolar field from a magnetic ion at site *j* to the nucleus at site *i* can be calculated numerically by using the formula,

$$\boldsymbol{H}_{\mathrm{dip}}(i,j) = \left[3\frac{(\bar{\boldsymbol{m}}_j\cdot\boldsymbol{r}_{ij})\boldsymbol{r}_{ij}}{r_{ij}^5} - \frac{\bar{\boldsymbol{m}}_j}{r_{ij}^3}\right], \tag{4}$$

where r_{ij} is the distance between sites *i* and *j*, and $\bar{\boldsymbol{m}}_j$ is the time average moment of Am along $\boldsymbol{H}_0$. The total $\boldsymbol{H}_{\mathrm{dip}}$ is obtained by summing over all the contributions from magnetic moments in the crystal. Using Eqs. (3) and (4), we simulated the ^{17}O NMR line

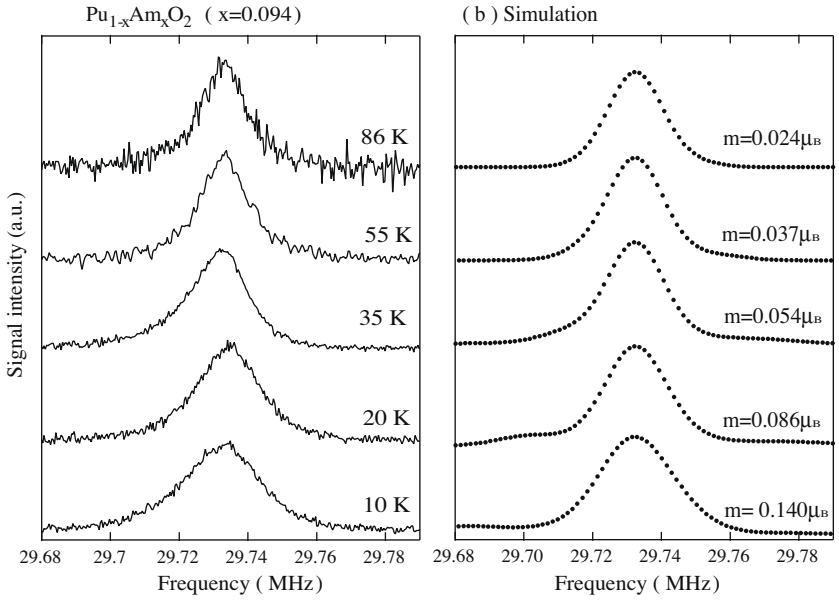

Fig. 1. (a) A series of ^{17}O NMR spectra for $(Pu_{0.91}Am_{0.09})O_2$ obtained with $H_0 = 51.51$ kOe at temperatures 10, 20, 35, 55, and 86 K, respectively. (b) The corresponding NMR line simulations using estimated values of the Am moment m (see text).

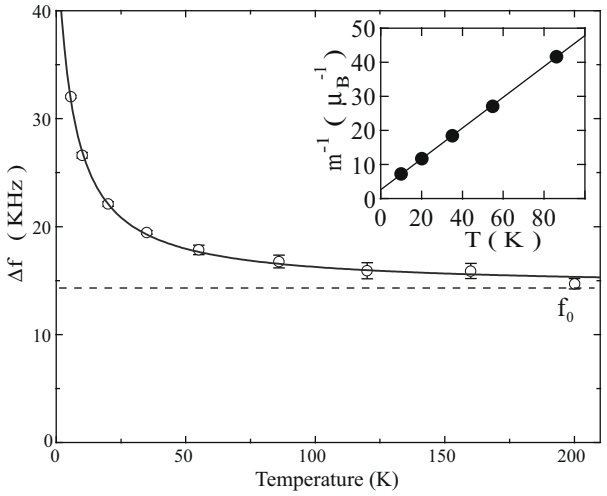

Fig. 2. The temperature dependence of the full width at half maximum of the NMR spectrum, Δf. The solid line shows the result of a least-squares fitting to Eq. (1). The dotted line represents the temperature independent part f_0. The inset shows the temperature dependence of m^{-1} estimated from the NMR line simulation at each temperature (see text). The solid line corresponds to the CW expression with an effective moment $\mu_{\rm eff} = 1.38\mu_B$ per Am ions.

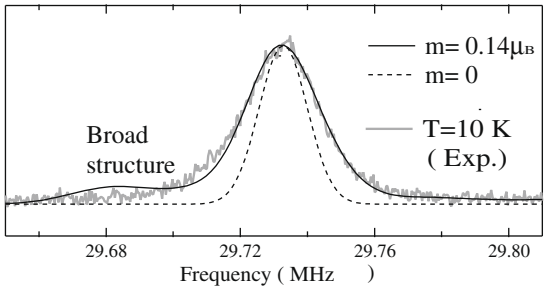

Fig. 3. An example of calculated envelope of the NMR spectrum with $m = 0.14\mu_B$ (solid line) and 0 (dotted line) along with experimental data at $T = 10$ K. (see text)

broadening due to the dipolar fields from the Am 5*f* moments in $(Pu_{0.91}Am_{0.09})O_2$. For this simulation, we took a PuO_2 cubic lattice consisting of 64 Pu and 128 O sites and randomly selected six Pu sites as Am sites (corresponds to ~9% substitution); we put $\bar{m}_j = m$ for Am sites, while $\bar{m}_j = 0$ for Pu sites. These numbers were determined in such a way that a further increase in the lattice sizes does not give any visible changes in the results. We calculated $\boldsymbol{H}_{\rm dip}$ for the eight oxygen sites located at the center of the cubic lattice, and then drew the histogram of their NMR frequencies f_N, where the direction of $\boldsymbol{H}_0$ was chosen randomly since we used a powder sample. The histogram was accumulated by repeating the calculation; each time the positions of Am ions on the lattice as well as the direction of $\boldsymbol{H}_0$ were chosen randomly. The calculation was repeated about 500 times until convergence of the result was obtained. Finally, in order to compare the results with experimental data, we took into account another source of broadening, i.e. the f_0 term in Eq. (1). A simple way to model the effect is to take a convolution with a Lorentzian broadening function of width f_0. If $f(x)$ is the histogram of the NMR frequencies and $g(y)$ the broadening function, the resulting envelope will be $F(y) = \int_{-\infty}^{+\infty} f(x)g(x-y)dx$.

In Fig. 3, we show the simulated envelope with $m = 0.14\mu_B$ along with experimental data at $T = 10$ K. For comparison, we also plot the envelope with $m = 0$ (no dipole interaction). Further examples of the simulations are also shown in Fig. 1b. The figures show that the nearly symmetric line broadenings at low temperatures are well reproduced by the simulations, which allowed us to estimate the magnetization per Am ion m at each temperature, as shown in Fig. 1b. In the inset of Fig. 2, we plot the temperature dependence of m^{-1} at $H_0 = 5.151$ T. The solid line corresponds to the CW expression with an effective moment $\mu_{\rm eff} = 1.38\mu_B$ per Am with $\theta = 5.8$ K. Note that the estimated value of $\mu_{\rm eff}$ is comparable with the values $\mu_{\rm eff} = 1.32$ or $1.53\mu_B$ per Am reported from $\chi(T)$ for AmO_2 [10].

It should be also noted that our NMR line simulations for $m > 0.08\mu_B$ show a broad structure at lower frequencies, as shown in Fig. 3. This broad structure originates from the ^{17}O sites adjacent to the Am ions. In the experiment, however, no such structure has been observed even at the lowest temperature of 10 K. We expect that the relaxation times of these adjacent O sites may be too short

to detect their NMR signals, since they are strongly coupled with the Am 5*f* moments. Further experimental effort is needed to clarify this point.

3.2. Nuclear spin–lattice relaxation

NMR can probe the dynamical property of a electron system via the nuclear spin–lattice relaxation measurements. The relaxation rate $1/T_1$ is related to the low-energy spin-fluctuation densities perpendicular to the quantization axis. Experimentally, $1/T_1$ is determined by fitting the nuclear recovery $p(t) \equiv [M(\infty) - M(t)]/M(\infty)$ to a theoretical function, where t is the time after a saturation pulse to the observation pulses and $M(t)$ is the nuclear magnetization. In the pure PuO_2, $p(t)$ for the ^{17}O nuclei shows an exponential time dependence, that is, $p(t) = p(0)\exp[-(t/T_1)]$ [6]. This is a characteristic of the nuclear spin system where there is no quadrupole splitting and no dispersion of $1/T_1$ among nuclei. In $(Pu_{0.91}Am_{0.09})O_2$, on the other hand, we have observed a nonexponential $p(t)$ in the whole temperature range studied. An example of the $p(t)$ curves is shown in Fig. 4. The nonexponential decay reveals that there is a distribution in $1/T_1$ over nuclei depending on the distance (r) from dilute relaxation sources.

The solid line in Fig. 4 shows the result of a least-squares fit to a product function, that is,

$$p(t) = p(0)\exp[-t/T_{1,\mathrm{host}} - (t/\tau)^{\beta}], \tag{5}$$

where $p(0)$, β and $1/\tau$ are fit parameters. The product function of Eq. (5) is widely applicable to systems containing magnetic impurities [23,24], where the $1/T_{1,host}$ is the nuclear relaxation rate of the host system, while the $1/\tau$ represents the relaxation process induced by the magnetic impurities. Here the values of $1/T_{1,host}$ were estimated from the $1/T_1$ of PuO_2. The temperature variation of the exponent β is shown in the inset of Fig. 4, where approximately $\beta \sim 0.5$ is obtained in the whole temperature range. Note that the $\beta \sim 0.5$ has been predicted for diffusionless relaxation process associated with the dipolar or Ruderman–Kittel–Kasuya–Yoshida (RKKY) interactions with dilute impurities, where the nuclear relaxation rate decays as $1/T_{1,\mathrm{imp}}(r) = \alpha/r^6$ [23,24]. $1/\tau$ is related with α by

$$(1/\tau)^{1/2} = \frac{4}{3}\pi^{3/2} c N_0 \alpha^{1/2}, \tag{6}$$

where c is the ratio of magnetic to non-magnetic sites and N_0 is the Avogadro number.

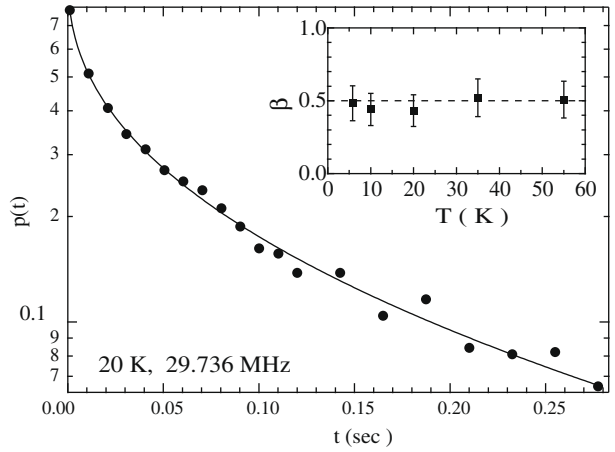

Fig. 4. An example of the observed $p(t)$ curves in $(Pu_{0.91}Am_{0.09})O_2$. The solid line shows the result of a least-squares fit to Eq. (5). The inset shows the temperature variation of the exponent β.

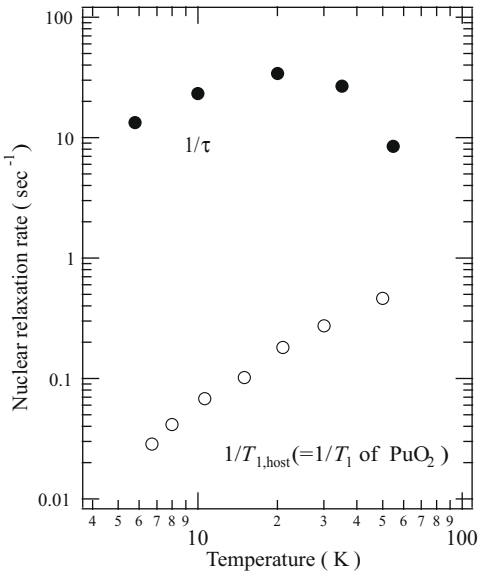

Fig. 5. The temperature dependence of the $1/\tau$ and $(1/T_1)_{\mathrm{host}}$ in $(Pu_{0.91}Am_{0.09})O_2$.

In Fig. 5, we plot the temperature dependence of $1/\tau$ and $1/T_{1,\mathrm{host}}$. Here $1/T_{1,host}$ is estimated from $1/T_1$ of PuO_2. In the whole temperature range, $1/\tau$ is more than an order magnitude larger than $1/T_{1,host}$. This reveals that the ^{17}O nuclear relaxation is dominated by the Am 5*f* moment fluctuations in $(Pu_{0.91}Am_{0.09})O_2$. In addition, $1/\tau$ increases with decreasing temperature and shows a broad maximum around 20 K. At present, the origin of the broad maximum is uncertain. However, we expect that the $1/\tau$ maximum may be associated with the slowing down of Am moment fluctuations at low temperature. In the presence of the moment fluctuations with a characteristic frequency ω_{fl}, $\alpha(\propto 1/\tau)$ is given by [25],

$$\alpha \sim (\gamma_N \bar{m}_j)^2 \frac{\omega_{\mathrm{fl}}}{\omega_{\mathrm{fl}}^2 + \omega_{\mathrm{res}}^2} \tag{7}$$

where ω_{res} is the resonance frequency of observation (~30 MHz). When $\omega_{\mathrm{fl}} \gg \omega_{\mathrm{res}}$ at high temperatures, α will be temperature-independent at $\sim (\gamma_N \bar{m}_j)^2/\omega_{\mathrm{fl}}$. At lower temperatures, on the other hand, α will be enhanced with decreasing ω_{fl}, and show a maximum at $\omega_{\mathrm{fl}} \simeq \omega_{\mathrm{res}}$. We suggest that the foregoing scenario may be tested by measuring the c and ω_{res} dependences of $1/\tau$. From Eqs. (6) and (7), $1/\tau$ is expected to have linear relations with c^2 and ω_{res}^{-2}. These experiments are now in preparation.

4. Summary

We have initiated the first ^{17}O NMR study on $(Pu_{0.91}Am_{0.09})O_2$. A temperature-dependent NMR line broadening has been observed at low temperatures. This result is well understood in terms of classical dipolar hyperfine fields from the 5*f* moments of the Am ions. By comparing the results of NMR line simulations with the experimental data, we have estimated the effective moment of the Am ions to be $\mu_{\mathrm{eff}} = 1.38\mu_B$. This value is comparable with $\mu_{\mathrm{eff}} = 1.32$ or $1.53\mu_B$ per Am in AmO_2. We have also measured the nuclear spin–lattice relaxation of ^{17}O. The ^{17}O nuclear magnetization recovery was found to show a nonexponential time dependence with the exponent $\beta \sim 0.5$. This effect has been identified as a relaxation process induced by Am moment fluctuations via dipolar hyperfine fields.

Acknowledgments

We thank M. Akabori and M. Takano for useful advice with sample preparation. We also thank R.E. Walstedt for valuable comments and discussions. A part of this study is the result of Basic actinide chemistry and physics research in close cooperation with hot laboratories carried out under the Strategic Promotion Program for Basic Nuclear Research by the Ministry of Education, Culture, Sports, Science and Technology of Japan.

References

[1] K. Ikushima, S. Tsutsui, Y. Haga, H. Yasuoka, R.E. Walstedt, N.M. Masaki, A. Nakamura, S. Nasu, Y. Ōnuki, Phys. Rev. B 63 (2001) 104404.
[2] Y. Tokunaga, Y. Homma, S. Kambe, D. Aoki, H. Sakai, E. Yamamoto, A. Nakamura, Y. Shiokawa, R.E. Walstedt, H. Yasuoka, Phys. Rev. Lett. 94 (2005) 137209.
[3] Y. Tokunaga, Y. Homma, S. Kambe, D. Aoki, H. Sakai, E. Yamamoto, A. Nakamura, Y. Shiokawa, R.E. Walstedt, H. Yasuoka, Physica B 359-361 (2005) 1096.
[4] Y. Tokunaga, D. Aoki, Y. Homma, S. Kambe, H. Sakai, S. Ikeda, T. Fujimoto, R.E. Walstedt, H. Yasuoka, E. Yamamoto, A. Nakamura, Y. Shiokawa, Phys. Rev. Lett. 97 (2006) 257601.
[5] Y. Tokunaga, Y. Homma, S. Kambe, D. Aoki, H. Sakai, E. Yamamoto, A. Nakamura, Y. Shiokawa, R.E. Walstedt, H. Yasuoka, Physica B 378–380 (2006) 929.
[6] Y. Tokunaga, H. Sakai, T. Fujimoto, S. Kambe, R.E. Walstedt, K. Ikushima, H. Yasuoka, D. Aoki, Y. Homma, Y. Haga, T.D. Matsuda, S. Ikeda, E. Yamamoto, A. Nakamura, Y. Shiokawa, K. Nakajima, Y. Arai, Y. Ōnuki, J. Alloys Compd. 444–445 (2007) 241.
[7] R.E. Walstedt, S. Kambe, Y. Tokunaga, H. Sakai, J. Phys. Soc. Jpn. 76 (2007) 072001.
[8] Y. Tokunaga, Y. Homma, S. Kambe, D. Aoki, H. Sakai, H. Chudo, K. Ikushima, E. Yamamoto, A. Nakamura, Y. Shiokawa, R.E. Walstedt, H. Yasuoka, J. Optoelectron. Adv. Mater. 10 (2008) 1663.
[9] Y. Tokunaga, R.E. Walstedt, Y. Homma, D. Aoki, S. Kambe, H. Sakai, T. Fujimoto, S. Ikeda, E. Yamamoto, A. Nakamura, Y. Shiokawa, H. Yasuoka, Phys. Rev. B 74 (2006) 064421.
[10] D.G. Karraker, J. Chem. Phys. 63 (1975) 3174.
[11] G.M. Kalvius, S.L. Rudy, B.D. Dunlap, G.K. Shenoy, D. Cohen, M.B. Brodsky, Phys. Lett. B 29 (1969) 489.
[12] A. Bœuf, J.M. Fournier, J.F. Gueugnon, L. Manes, J. Rebizant, F. Rustichelli, Le J. de Phys. 40 (1979) L–335.
[13] M. Osaka, H. Serizawa, M. Kato, K. Nakajima, Y. Tachi, R. Kitamura, S. Miwa, T. Iwai, K. Tanaka, M. Inoue, Y. Arai, J. Nucl. Sci. Technol. 44 (3) (2007) 309.
[14] W. Maschek, X. Chen, F. Delage, A. Fernandez-Carretero, D. Haas, C. Matzerath Boccaccini, A. Rineiski, P. Smith, V. Sobolev, R. Thetford, J. Wallenius, Prog. Nucl. Energy 50 (2008) 333.
[15] M. Takano, M. Akabori, Y. Arai, K. Minato, J. Nucl. Mater. 376 (2008) 114.
[16] Y. Tokunaga, M. Osaka, S. Miwa, S. Kambe, H. Sakai, H. Chudo, and Y. Homma, unpublished.
[17] G.A. Candela, C.A. Hutchison, W.B. Lewis, J. Chem. Phys. 30 (1959) 246.
[18] G. Raphael, R. Lallement, Solid State Commun. 6 (1968) 383.
[19] S. Kern, R.A. Robinson, H. Nakotte, G.H. Lander, B. Cort, P. Watson, F.A. Vigil, Phys. Rev. B 59 (1999) 104.
[20] M. Colarieti-Tosti, O. Eriksson, L. Nordström, J. Wills, M.S.S. Brooks, Phys. Rev. B 65 (2002) 195102.
[21] N. Edelstein, H.F. Mollet, W.C. Easley, R.J. Mehlhorn, J. Chem. Phys. 51 (1969) 3281.
[22] T. Hotta, Phys. Rev. B 80 (2009) 024408.
[23] D. Tse, S.R. Hartmann, Phys. Rev. Lett. 21 (1968) 511.
[24] M.R. McHenry, B.G. Silbernagel, J.H. Wernick, Phys. Rev. Lett. 27 (1971) 426.
[25] A. Abragam, The Principles of Nuclear Magnetism, Oxford University Press, Oxford, 1961 (Chapter IX).